Supplementary material for:

Thermal expansion of liquid Fe-S alloy at high pressure

F. Xu[a,1], G. Morard[a,b] , N. Guignot[c], A. Rivoldini[d], G. Manthilake[e], J.Chantel[f], L. Xie[g,2], A. Yoneda[h], A. King[c], E. Boulard[a], S. Pandolfi[a,3], F. J. Ryerson[i], D. Antonangeli[a,*]

[a] Sorbonne Université, Muséum National d'Histoire Naturelle, UMR CNRS 7590, Institut de Minéralogie, de Physique des Matériaux et de Cosmochimie, IMPMC, 75005 Paris, France

[b] Université Grenoble Alpes, Université Savoie Mont Blanc, CNRS, IRD, Université Gustave Eiffel, ISTerre, 38000 Grenoble, France

[c] Synchrotron SOLEIL, L'Orme de Merisiers, Saint Aubin-BP48, 91192 Gif-sur-Yvette, France

[d] Royal Observatory of Belgium, Avenue Circulaire 3, B-1180 Brussels, Belgium

[e] Laboratoire Magmas et Volcans CNRS, IRD, OPGC, Université Clermont Auvergne, 63000 Clermont-Ferrand, France

[f] Univ. Lille, CNRS, INRAE, Centrale Lille, UMR 8207 - UMET - Unité Matériaux et Transformations, F-59000 Lille, France

[g] Institute for Planetary Materials, Okayama University, Misasa, Tottori 682-0193, Japan

[h] Department of Earth and Space Science, Graduate School for Science, Osaka University, Toyonaka, Osaka 560-0043, Japan

[i] Lawrence Livermore National Laboratory, 7000 East Avenue, Livermore, California 94550-9698, U.S.A

[1] Currently at Department of Earth Sciences, University College London, WC1E 6BT London, United Kingdom

[2] Currently at Bayerisches Geoinstitut, Universität Bayreuth, 95440 Bayreuth, Germany

[3] Currently at Fundamental Physics Directorate, SLAC National Accelerator Laboratory, Menlo Park, CA, United States

*Corresponding author.

E-mail: daniele.antonangeli@upmc.fr

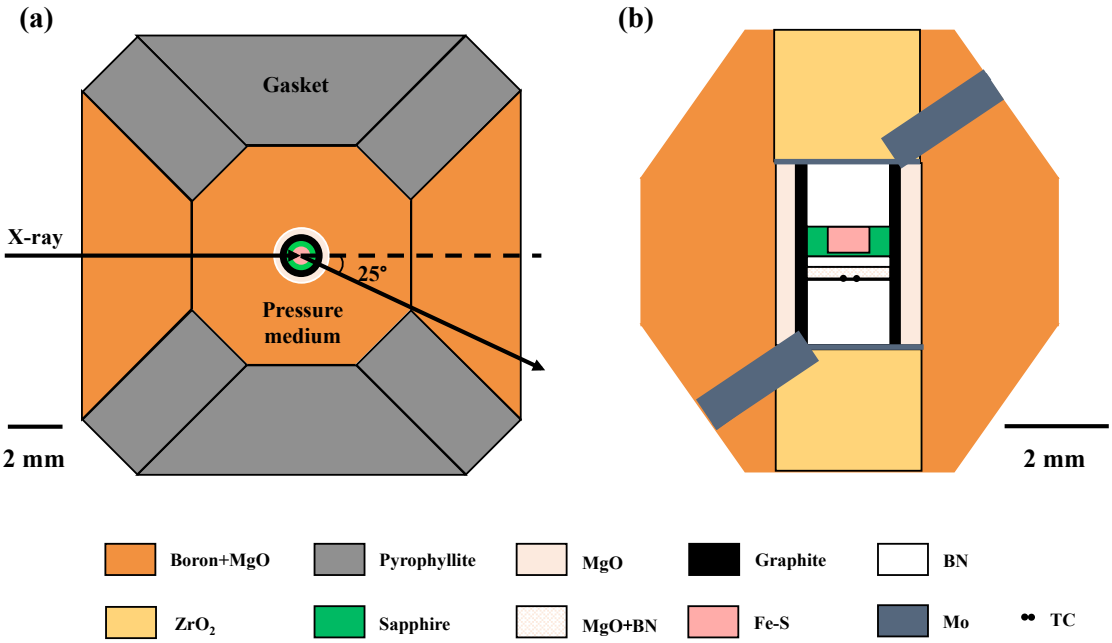

Fig. S1 Schematic illustration of the experimental design. (a) A top view of the diffraction geometry through the gasket and cell assembly. (b) A cross-section of cell assembly used in this study. Temperature was monitored with a $W_{97}Re3$-$W_{75}Re_{25}$ thermocouple (TC) whose junction was indicated by black dots.

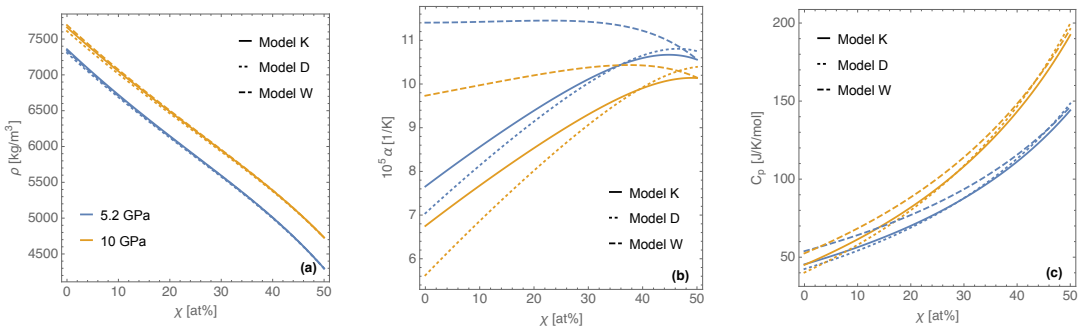

Fig.S2. Density (a), thermal expansivity (b), and iso-baric heat capacity (c) as a function of molar sulfur fraction X at 5.2 GPa and 10 GPa and 2000K for the thermodynamic Model K, Model D and Model W. Model K, Model D and Model W differ in the reference EOS for liquid iron (Model K uses l-Fe EOS of Komabayashi (2014), Model D uses l-Fe EOS of Dorogokupets et al. (2017), Model W uses l-Fe EOS of Wagle and Steinle-Neumann (2019)). Parameters of the thermodynamic models are in Table S1 and S2.

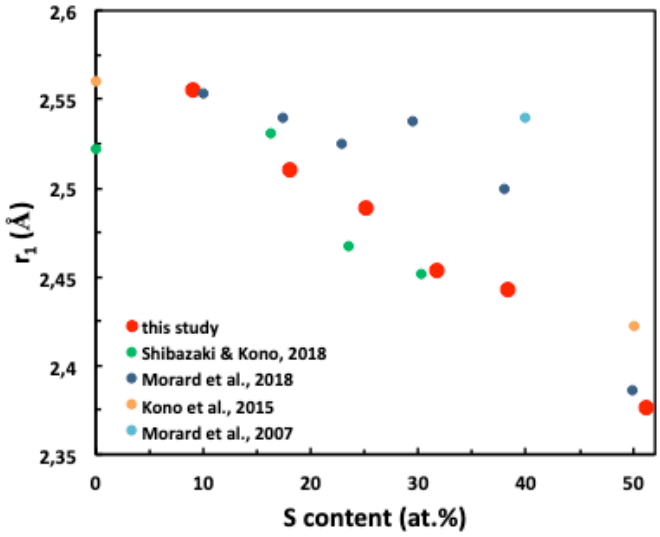

Fig.S3. First peak position (r_1) as a function of the S content. Previous results from Shibazaki et al. (2018) at 3-5 GPa, Morard et al. (2018) at 2-5 GPa, Kono et al. (2015) at 1-6 GPa, and Morard et al. (2007) at 3-17 GPa, were also shown for comparison. For clarity only one value is plotted for each of the considered composition (r_1 for a given S content only moderately depends on pressure and temperature over the P-T range covered by individual studies).

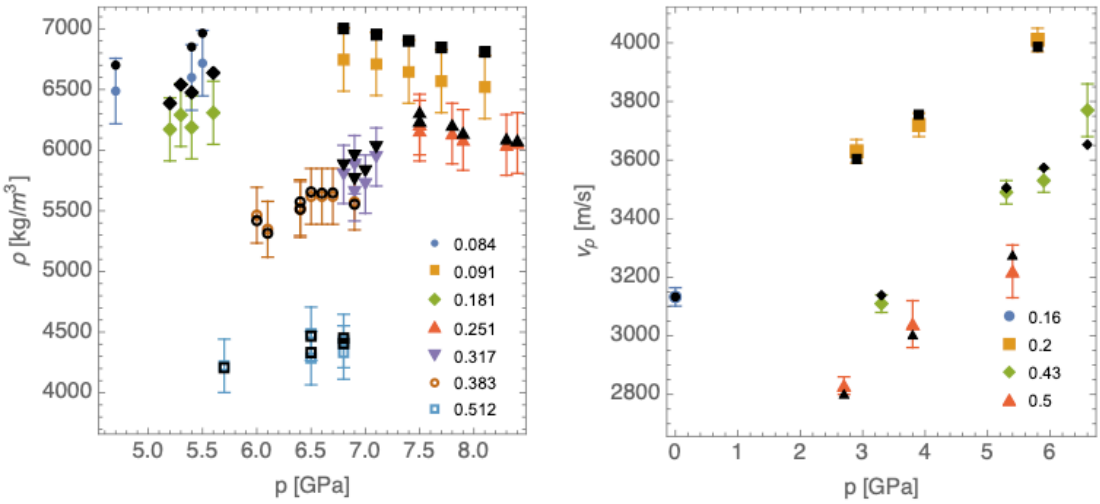

Fig. S4. Measured densities (this study) and acoustic velocities (Nasch et al. 1994 and Nishida et al. 2016) (colored symbols) at varying temperature and predicted values according to the thermodynamic Model W (black symbols) under the same condition. Different symbols corresponds to different S content. For details on the thermodynamic model, please refer to section 2.5 and to Table S1 and S2 for parameters.

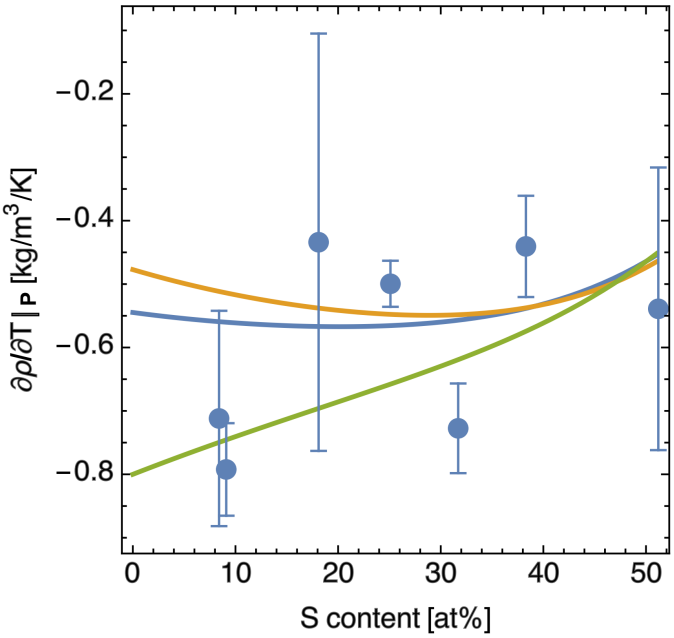

Fig. S5. Temperature derivatives at the constant pressure (7 GPa) of density as a function of S content. Dots are the slopes of the linear fit to the experimental data (see Fig. 6) with uncertainties at 2σ. Colored lines are outcomes of thermodynamic Model K (blue), Model D (orange) and Model W (green). Model K, Model D and Model W differ in the reference EOS for liquid iron (Model K uses l-Fe EOS of Komabayashi (2014), Model D uses l-Fe EOS of Dorogokupets et al. (2017), Model W uses l-Fe EOS of Wagle and Steinle-Neumann (2019)). Parameters of the thermodynamic models are in Table S1 and S2.

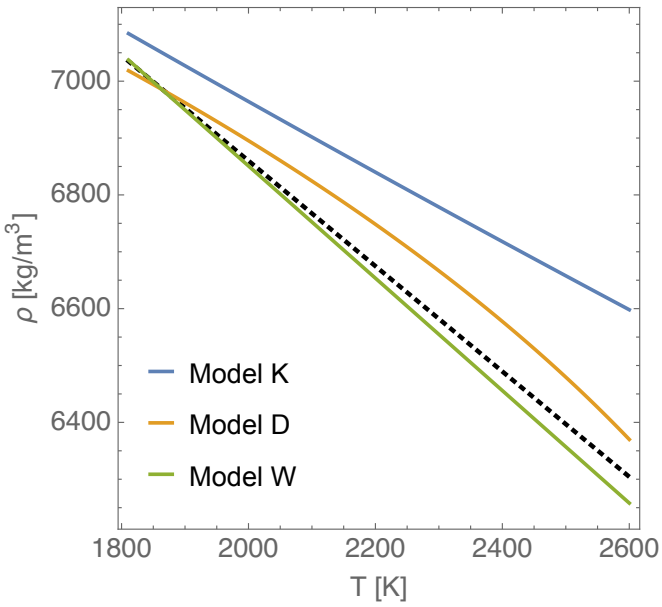

78

79

80 **Fig. S6.** Density as a function of temperature for liquid iron at ambient pressure. Colored
81 lines are outcomes of our thermodynamic models (see section 2.5 and Table S1 and S3 for
82 details). Dashed black line is a fit to data from Assael et al.. (2006), and preferred fit
83 according to Williams (2009).

84

85

86 **Table S1**. EOS parameters for l-FeS and Margules parameters estimated from the
87 experimental data of this study and from density measurements of Morad et al. (2018) and
88 acoustic velocities from Nishida et al. (2016) using the EOS of l-Fe of Komabayashi (2014),
89 Model K, Dorogokupets et al. (2017), Model D and Wagle and Steinle-Neumann (2019),
90 Model W. $P_{ref} = 0.1$MPa, $T_{ref} = 1650$ K and for the l-FeS end-member $\kappa = 1.4$,
91 $\alpha = 11.8 \times 10^{-5}$1/K, and $C_p = 62.5$ J/K/mol.

92

Thermodynamic model	l-Fe EOS	V [cm^3/ mol]	K_T [GPa]	$K_T{}'$	γ	δ_T	W_{Fe}	W_{FeS}	B_0 [GPa]	B'
Model K	Komabayashi 2014	24.25	13.22	6.36	0.68	0.62	-9.627	-3.435	3.45	2.14
Model D	Dorogokupets 2017	24.26	13.12	6.38	0.68	0.52	-9.481	-3.528	3.44	2.10
Model W	Wagle 2019	24.26	13.07	6.44	0.68	0.61	-9.627	-3.393	3.44	2.23

93

94

95 **Table S2**. Margules parameters required to compute the Fe-S liquidus (see Eq. 9-11
96 Buono et al. 2011) for the EOS' of l-Fe of Komabayashi (2014) and Dorogokupets et al.
97 (2017). For the Model W the EOS' of solid Fe from Komabayashi (2014) has been used to
98 compute the slope of the liquidi.

99

Thermodynamic model	l-Fe EOS	$W_{H,Fe}$ [kJ/mol]	$W_{S,Fe}$ [kJ/mol/K]	$W_{V,Fe}$ [kJ/mol/ GPa]	$W_{H,FeS}$ [kJ/mol]	$W_{H,FeS}$ [kJ/mol/K]	$W_{H,FeS}$ [kJ/mol/GPa]
Model K	Komabayashi 2014	53.70	0.029	-3.82	25.34	0.0	-2.95
Model D	Dorogokupets 2017	69.28	0.043	-2.78	27.3	0.0	-3.48

100

101